

Effects of dislocations on electron transport in wurtzite InN

Xin-Gang Yu and Xin-Gang Liang^{a)}

Department of Engineering Mechanics, Heat Transfer and Energy Conversion—The Key Laboratory of Beijing Municipality, Tsinghua University, Beijing 100084, China

(Received 17 August 2007; accepted 3 December 2007; published online 25 February 2008)

A semiclassical three-valley Monte Carlo simulation approach was used to investigate electron transport in bulk InN using a revised set of material parameters. The simulation accounted for acoustic phonons, polar optical phonons, ionized impurities, and piezoelectric and dislocation scattering. The main emphasis is to analyze the effect of dislocations on the electron drift velocity and drift mobility. At low electric field strengths, dislocations have a significant impact on the steady and transient electron drift velocities. However, at high electric field strengths, the effects of dislocations on the drift velocity can be neglected. The electron mobility in InN with structural defects has a critical dislocation density below which dislocations have no effect on the mobility and beyond which the increased dislocation density results in an order-of-magnitude decrease in the electron mobility in InN. © 2008 American Institute of Physics. [DOI: 10.1063/1.2840051]

I. INTRODUCTION

Interest in indium nitride, an important III–V compound semiconductor with many potential applications, has mushroomed recently.¹ The use of InN and its alloys with GaN and AlN makes it possible to extend the emissions of nitride-based light-emitting diodes (LED) and laser diodes (LD) from the ultraviolet to the near-infrared region.² Moreover, InN is predicted to have the lowest effective mass for electrons of all the III-nitride semiconductors, which leads to a high mobility and a high saturation velocity as well as a high peak overshoot velocity.³ Consequently, InN is expected to be used for the fabrication of high-frequency transistors operating at high powers and temperatures due to its potentially superior performance over other III-nitrides.

These applications will require high-quality InN with a high degree of structural integrity and good optical and electrical properties. However, the growth of InN crystals presents a challenge because of the lack of a suitable substrate. So far, the most extensively used substrate material for the epitaxial growth of InN has been sapphire (Al_2O_3), which has a lattice mismatch of $\sim 25\%$ with InN. This large lattice mismatch and the thermal expansion coefficient difference can result in a high concentration of threading edges and screw dislocations which traverse perpendicularly from the InN/ Al_2O_3 interface to the InN surface. The dislocation line in this area is known to be negatively charged.^{4,5} Accordingly, it acts as a line of Coulomb scattering centers which influences the electrical properties of the material.

Although many properties of InN have been studied since the 1980s, some are still far from being fully understood. For example, for a long time wurtzite InN has thought to be a wide band gap material with a band gap of about 2.0 eV. However, recent experimental and theoretical investigations have provided convincing evidence that the band gap of InN is actually about 0.7 eV.^{6,7} Consequently, previous simu-

lations of electron transport in InN appear to be inaccurate since they were based on a conduction band structure that recent experimental data have shown to be inaccurate. Accordingly, there have been many studies to re-examine the transport properties of InN. Bulutay and Ridley⁸ obtained the steady-state velocity-field characteristics of InN using an ensemble Monte Carlo technique based on more reliable band structure data. O'Leary *et al.*⁹ used a semiclassical Monte Carlo simulation approach to analyze the steady-state and transient electron transport within bulk wurtzite InN with the updated band structure. Then, Polyakov *et al.*¹⁰ used the ensemble Monte Carlo method to study steady-state and transient electron transport in bulk wurtzite InN for various electric fields and temperatures based on the refined conduction band structure. Polyakov and Schwierz¹¹ analyzed the low-field electron mobility in bulk wurtzite InN at room temperature over a wide range of carrier concentrations using the ensemble Monte Carlo method. However, these simulations all neglected the effects of dislocations. The optimization of electronic devices based on InN requires a detailed knowledge of the electronic properties of InN, especially the effects of structural defects which are electrically active and affect the drift velocity, mobility, and free-carrier concentrations. As a consequence, the effects of dislocations must be taken into account when analyzing the InN transport properties.

At present, there are no theoretical analyses of the transport properties of InN with structural defects. In this work the ensemble Monte Carlo (MC) method is used to investigate electron transport in bulk wurtzite InN based on the refined band structure. The analyses study the effects of dislocations on the electron drift velocity and low-field mobility.

II. MODEL DESCRIPTION

This analysis used a multivalley approximation to the band structure that accounts for the three lowest conduction band minima with nonparabolicity. The parameters for the

^{a)}Author to whom correspondence should be addressed. Telephone: +86-10-6278-8702. Electronic mail: liangxg@tsinghua.edu.cn.

TABLE I. InN Material parameters (Ref. 16).

Parameter	InN
Mass density (g/cm ³)	6.81
Longitudinal sound velocity (cm/s)	6.24×10^5
Transverse sound velocity (cm/s)	2.55×10^5
Acoustic deformation potential (eV)	7.1
Static dielectric constant	15.3
High-frequency dielectric constant	8.4
Piezoelectric constant	3.75×10^{-5}
Optical phonon energy (meV)	89
Intervalley deformation potentials (eV/cm)	10^9
Intervalley phonon energies (meV)	89

valleys given in Table I are from recent band structure calculations.¹¹ Kane's model¹¹ is used to estimate the nonparabolicity of the valleys. The satellite valleys Γ_3 and $M-L$ are assumed to be parabolic (i.e., $\alpha=0$), while the main Γ_1 valley is assumed to not be parabolic. This valley can be fit well by

$$\frac{\hbar^2 k^2}{2m^*} = E(1 + \alpha E), \quad (1)$$

where \hbar is the reduced Planck's constant, k is the electron wave vector, m^* is the effective mass, α is a nonparabolicity parameter, and E is the electron energy.

The scattering mechanisms in the simulations include polar optical phonons, ionized impurities, the deformation potential, piezoelectric acoustic phonons, and intervalley and dislocation scattering that were ignored in former MC simulations. The interactions of electrons with ionized impurities is treated using modified a Brooks-Herring approach,¹² which considers the electron degeneracy.

The dislocations affect electron transport in InN not only through Coulomb interactions of electrons with charged dislocation cores, but also through the induced lattice strain surrounding dislocations.¹³ Strain field scattering will affect low-temperature transport properties when the electron density is low and the dislocation density is high. In the present work, as in previous studies,^{14,15} the effect of strain fields was neglected to simplify the simulation since the carrier density is large and the dislocation density is not quite as huge. The agreement of the calculation in Ref. 14 with the experimental result justifies this treatment. Any electrons moving near a negatively charged dislocation line will be scattered. The scattering by dislocations is modeled as described by Look and Sizelove,¹⁵

$$\frac{1}{\tau_{\text{dis}}} = \frac{\hbar^3 \varepsilon^2 c^2 (1 + 4\lambda^2 k_{\perp}^2)^{3/2}}{N_d m^* e^4 \lambda^4}, \quad (2)$$

where ε is the static dielectric constant, c is the lattice constant along the [001] direction, N_d is the dislocation density, k_{\perp} is the component of the electron wave vector k perpendicular to the direction of the dislocation, and λ is the Debye length, defined as

$$\lambda = (\varepsilon k_B T / e^2 n)^{1/2}, \quad (3)$$

where k_B is Boltzmann's constant, T is the temperature in Kelvin, e is the electron charge, and n is the free-electron

TABLE II. InN band structure parameters (Ref. 11).

Valley number	1	2	3
Valley location	Γ_1	Γ_2	$L-M$
Valley degeneracy	1	1	6
Effective mass	0.04	0.25	1
Intervalley energy separation (eV)	0	1.775	2.709
Energy gap (eV)	0.7		
Nonparabolicity (eV ⁻¹)	1.43	0	0

density, which can be determined from the charge balance equation. The values for the various constants which determine the scattering rates are presented in Table II.¹⁶ The dislocation scattering is an elastic interaction without loss or gain of energy, and the effect of the dislocation direction on the mobility was neglected in the simulation. Since the interaction of the free electron and dislocation line is Coulomb interaction, θ between the wave vector before and after the scattering can be determined within the framework of the Brooks-Herring theory by application of the direct technique. The degeneracy effects are incorporated using the rejection technique.

Using the relation $\mu = v_{\text{drift}}/E$, the low-field mobility is obtained from a straight line fit of the velocity-electric field curve at low electric field strengths. In MC calculational statistics, the simulations used an electron number of 10^4 , a time step of 2 fs, and a simulation time of 1.6×10^3 ps.

III. RESULTS AND DISCUSSION

Figure 1 shows the steady-state electron drift velocity in wurtzite InN calculated as a function of the applied electric field strength with and without dislocations for a crystal temperature of 300 K. the ionized impurity concentration is equal to 10^{17} cm⁻³. The calculated drift velocity for InN without dislocations agrees well with previous Monte Carlo simulations,^{9,11} which validates the code. The effects of dislocations on the steady-state electron drift velocity can be divided into two parts relative to the field strength that gives the maximum drift velocity. In low strengths less than the

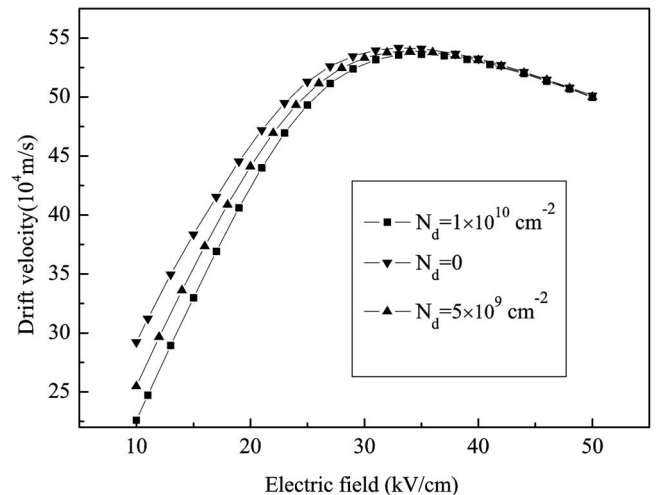


FIG. 1. Drift velocities for various electric field strengths and dislocation concentrations.

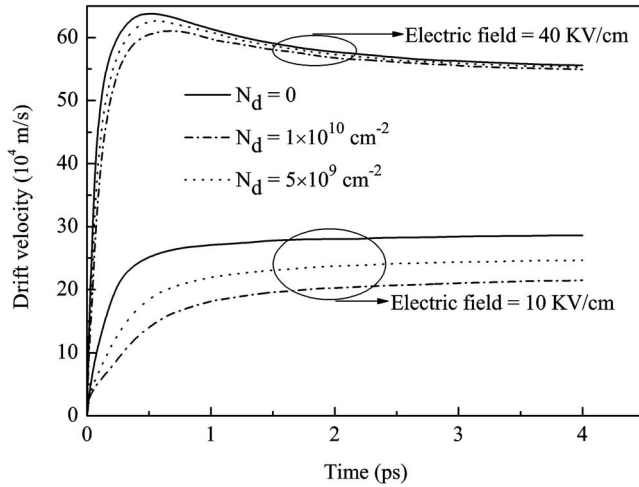


FIG. 2. Transient drift velocities at 40 and 10 kV/cm.

peak, the influence of the dislocation scattering is significant, i.e., the dislocation line drastically reduces the steady-state electron drift velocity. However, with increasing electric strength, the effects of dislocations decrease. For electric field strengths in excess of 35 kV/cm, the dislocation scattering has little impact on the electron drift velocity, as intervalley and polar optical scattering play more important roles in the scattering.

The effects of dislocations on the transient drift velocity of InN are shown in Fig. 2 for electric fields of $E=40$ and $E=10$ kV/cm at a temperature of 300 K. The ionized impurity concentration is set to be 10^{17} cm $^{-3}$. As shown in Fig. 2, at $E=40$ kV/cm the drift velocity overshoots the steady-state value within about 0.5 ps. The velocity overshoot is moderated and delayed by the dislocation scattering. The total scattering rate is higher with dislocation scattering and, thus, a longer time is required to heat the carriers prior to the onset of the overshoot. Consequently, dislocations will impact on the performance of high-speed devices based on wurtzite InN. By comparison, the transient velocities at electric field strengths less than the values that cause velocity overshoot (~ 35 kV/cm) are also shown in Fig. 2. The transient drift velocity at low field strengths is significantly reduced by dislocation scattering with no velocity overshoot.

There will be a significant dislocation effect on the low-field strength mobility because the scattering of the dislocation line significantly influences the low-field strength drift velocity. The calculations were calibrated by comparing the results to previous experimental studies of electron mobility in wurtzite InN. Wang *et al.*¹⁷ reported on the transport properties of high-quality InN epitaxy films grown on GaN substrates. The electron mobilities of four samples for room temperature (300 K) and 77 K are listed in Table III with calculated results using the present model. Because not all dislocations will be charged, the dislocation density was chosen as a fitting number and a value of $N_d=1 \times 10^{11}$ cm $^{-2}$ was used to best fit the experimental data. To compare with measured results, the ionized impurity concentration in the simulation is chosen according to the bulk charge balance equation,

TABLE III. Comparison of measured and predicted mobilities.

Sample	RT mobility (cm 2 /Vs)		77 K mobility (cm 2 /Vs)	
	Measured (Ref. 17)	Calculated	Measured (Ref. 17)	Calculated
A	943	983.9	1009	1230
B	782	987.2	809	1224.9
C	1054	997	1154	1221.3
D	984	990	1036	1223

$$N_{D_{\text{on}}} = n + N_A + N_d/c, \quad (4)$$

where $N_{D_{\text{on}}}$ is the doping concentration, N_A is the corresponding acceptor density, n is the free-carrier density. N_A and n are set to be the same as the four samples in Ref. 17.

The measured mobilities for these samples varied from 782 to 1054 cm 2 /Vs at room temperature and from 809 to 1154 at 77 K due to differences in the specimen. The theoretical results agree well with the measured values. Note that the calculated values give the drift mobility, whereas the experimental results are the Hall mobility. Since the Fermi level in the simulations is above the conduction band edge, the carriers are degenerate. Therefore, the Hall mobility and the drift mobility are identical.

The effect of structural defects on the low-field strength electron mobility in bulk InN at 300 K is shown in Fig. 3 as a function of the dislocation concentration. The doping concentration and corresponding acceptor density were set to be 5×10^{18} and 5×10^{17} cm $^{-3}$, respectively, in the simulation. In Fig. 3, as the dislocation density exceeds $N_D=10^9$ cm $^{-2}$, the low-field strength mobility starts to decrease. In the range of $N_D=10^9$ – 10^{11} cm $^{-2}$, the room-temperature mobility is strongly dependent on the dislocation line density with a decrease from 1800 cm 2 /Vs at 10^9 cm $^{-2}$ to 950 cm 2 /Vs at 10^{11} cm $^{-2}$. For low dislocation densities ($N_D < 10^9$ cm $^{-2}$), the room-temperature mobility does not depend on N_D but is determined by other scattering mechanisms, i.e., polar optical phonons, ionized impurity, and so on. It is astounding to most observers that optical devices such as LEDs and LDs based on III-nitride will work well with such a high dislocation density since, in GaAs-based LDs, a value of N_d

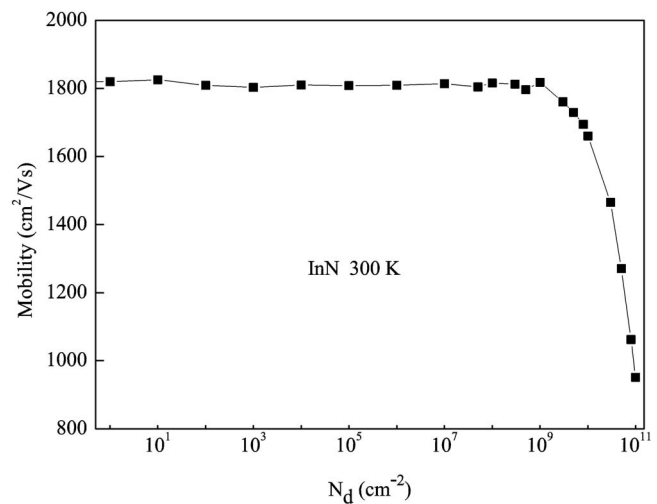


FIG. 3. Mobility in InN for various dislocation concentrations at 300 K.

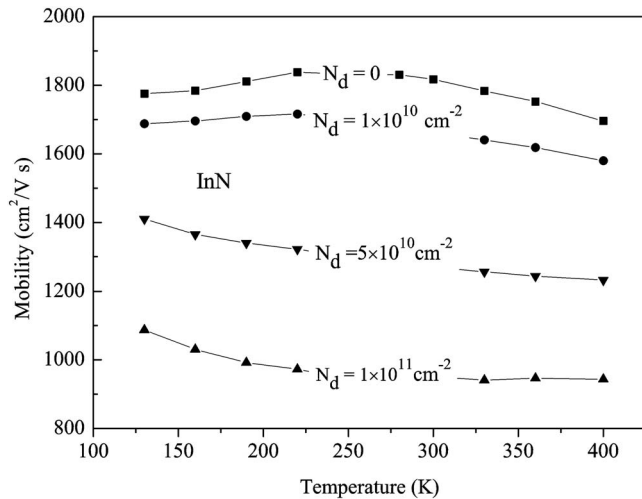


FIG. 4. Mobility in InN for various temperatures and dislocation concentrations.

$= 10^4 \text{ cm}^{-2}$ is usually sufficient to prevent laser action.¹⁸ That the mobility of nitride is insensitive to the dislocation concentration for N_d less than a critical value such as 10^9 cm^{-2} in InN may be part of the reason.

The numerically calculated electron mobility is shown in Fig. 4 as a function of the temperature for various dislocation concentrations for the same doping concentration and acceptor concentration as before. Figure 4 clearly shows that, with increasing the dislocation density, the low-field strength mobility decreases significantly over a wide temperature range. The low-field strength mobility $\mu(N_d, 300 \text{ K})$ changes from $1800 \text{ cm}^2/\text{Vs}$ without dislocations to $950 \text{ cm}^2/\text{Vs}$ with a dislocation density of 10^{11} cm^{-2} . In addition, the variation of the electron mobility with temperature changes. For dislocation concentrations less than 10^{10} cm^{-2} , the mobility increases with the increasing temperature to a peak at about 230 K, then decreases with increasing temperature, which qualitatively agrees with the temperature dependence of measured mobilities^{17,19} for InN and other nitrides. For dislocation densities in excess of $5 \times 10^{10} \text{ cm}^{-2}$, the mobility decreases linearly with increasing temperature in the range of 130–400 K, since free carriers are significantly reduced by the dislocation lines with increasing dislocation density. Thus, the material becomes nondegenerate, the relative importance of the scattering mechanisms changes with the dislocation scattering, and polar optical phonon scattering becoming dominant. Consequently, the low-field strength mobility decreases at elevated temperatures. At a low temperature below 150 K, a smaller electron energy makes impurity and acoustic phonon scatterings the dominant processes.²⁰ With a further decrease of the electron wave vector, piezoelectric scattering will become pronounced relative to other scattering channels.²¹ The low-field strength mobility will significantly depend on these mechanisms at a very low temperature.

IV. CONCLUSIONS

The effects of dislocations on electron transport in InN have been studied using Monte Carlo simulations. For applied electric field strengths in excess of 35 kV/cm , dislocation scattering has little impact on the electron drift velocity, as intervalley and polar optical scattering play the most important roles in the scattering. At low strengths, the effects of dislocations become significant. At room temperature, the low-field strength electron mobility in InN decreases drastically from $1800 \text{ cm}^2/\text{Vs}$ at 10^9 cm^{-2} to $950 \text{ cm}^2/\text{Vs}$ at 10^{11} cm^{-2} for $N_D = 10^9 - 10^{11} \text{ cm}^{-2}$ as the dislocation line density increases. For low dislocation densities ($N_d < 10^9 \text{ cm}^{-2}$), the room-temperature mobility does not depend on N_d .

Analysis of the temperature dependence of the electron mobility for various dislocation densities showed that both the magnitude and temperature dependence of the mobility are influenced by the dislocation lines.

ACKNOWLEDGMENTS

This work was supported by the National Natural Science Foundation of China (Grant No. 50376025).

- ¹S. K. O'Leary, B. E. Foutz, M. S. Shur, and L. F. Eastman, *Appl. Phys. Lett.* **88**, 152113 (2006).
- ²A. G. Bhuiyan, A. Hashimoto, and A. Yamamoto, *J. Appl. Phys.* **94**, 2779 (2003).
- ³S. N. Mohammad and H. Morkoc, *Prog. Quantum Electron.* **20**, 361 (1996).
- ⁴J. Elsner, R. Jones, M. I. Heggie, P. K. Sitch, M. Haugk, T. Frauenheim, S. Öberg, and P. R. Briddon, *Phys. Rev. B* **58**, 12571 (1998).
- ⁵P. J. Hansen, Y. E. Strausser, A. N. Erickson, E. J. Tarsa, P. Kozodoy, E. G. Brazel, J. P. Ibbetson, U. Mishra, V. Narayanamurti, S. P. DenBaars and J. S. Speck, *Appl. Phys. Lett.* **72**, 2247 (1998).
- ⁶A. A. Klochikhin, V. Y. Davydov, V. V. Emtsev, A. V. Sakharov, V. A. Kapitonov, B. A. Andreev, H. Lu, and W. J. Schaff, *Phys. Rev. B* **71**, 195207 (2005).
- ⁷I. Mahboob, T. D. Veal, L. F. J. Piper, C. F. McConville, H. Lu, W. J. Schaff, J. Furthmüller, and F. Bechstedt, *Phys. Rev. B* **69**, 201307 (2004).
- ⁸C. Bulutay and B. K. Ridley, *Superlattices Microstruct.* **36**, 465 (2004).
- ⁹S. K. O'Leary, B. E. Foutz, M. S. Shur, and L. F. Eastman, *Appl. Phys. Lett.* **87**, 222103 (2005).
- ¹⁰V. M. Polyakov, F. Schwierz, D. Fritsch, and H. Schmidt, *Phys. Status Solidi C* **3**, 598 (2006).
- ¹¹V. M. Polyakov and F. Schwierz, *Appl. Phys. Lett.* **88**, 032101 (2006).
- ¹²C. Moglestue, *Monte Carlo Simulation of Semiconductor Devices* (Chapman & Hall, London, 1993), p. 103.
- ¹³D. Jena and U. K. Mishra, *Appl. Phys. Lett.* **80**, 64 (2002).
- ¹⁴V. M. Polyakov and F. Schwierz, *J. Appl. Phys.* **101**, 033703 (2007).
- ¹⁵D. C. Look and J. R. Sizelove, *Phys. Rev. Lett.* **82**, 1237 (1999).
- ¹⁶S. K. O'Leary, B. E. Foutz, M. S. Shur, and L. F. Eastman, *J. Mater. Sci.: Mater. Electron.* **17**, 87 (2006).
- ¹⁷K. J. Wang, Y. Cao, J. Simon, J. Zhang, A. Mintairov, J. Merz, D. Hall, T. Kosel, and D. Jena, *Appl. Phys. Lett.* **89**, 162110 (2006).
- ¹⁸E. F. Schubert, *Light Emitting Diodes* (Cambridge University Press, Cambridge, 2003), p. 166.
- ¹⁹I. M. Abdel-Motaleb and R. Y. Korotkov, *J. Appl. Phys.* **97**, 093715 (2005).
- ²⁰A. F. M. Anwar, S. Wu, and R. T. Webster, *IEEE Trans. Electron Devices* **48**, 567 (2001).
- ²¹S. K. O'Leary, B. E. Foutz, M. S. Shur, and L. F. Eastman, *J. Mater. Sci.: Mater. Electron.* **17**, 87 (2006).